Correlation of Binding-Loop Internal Dynamics with Stability and Function in Potato I Inhibitor Family: Relative Contributions of Arg^{50} and Arg^{52} in *Cucurbita maxima* Trypsin Inhibitor-V As Studied by Site-Directed Mutagenesis and NMR Spectroscopy†

Mengli Cai,‡,§ Yu-Xi Gong,‡ Lisa Wen,⊥ and Ramaswamy Krishnamoorthi*,‡

Department of Biochemistry, Kansas State University, Manhattan, Kansas 66506, and Department of Chemistry, Western Illinois University, Macomb, Illinois 61455

Received March 29, 2002; Revised Manuscript Received May 22, 2002

ABSTRACT: The side chains of Arg^{50} and Arg^{52} at positions P_6' and P_8', respectively, anchor the binding loop to the protein scaffold by means of hydrogen bonds in *Cucurbita maxima* trypsin inhibitor-V (CMTI-V), a potato I family member. Here, we have investigated the relative contributions of Arg^{50} and Arg^{52} to the binding-loop flexibility and stability by determining changes in structure, dynamics, and proteolytic stability as a consequence of individually mutating them into an alanine. We have compared chemical shift assignments of main-chain hydrogens and nitrogens, and $^1H-^1H$ interresidue nuclear Overhauser effects (NOEs) for the two mutants with those of the wild-type protein. We have also measured NMR longitudinal and transverse relaxation rates and $^{15}N-^1H$ NOE enhancements for all backbone and side-chain NH groups and calculated the model-free parameters for R50A-rCMTI-V and R52A-rCMTI-V. The three-dimensional structures and backbone dynamics of the protein scaffold region remain very similar for both mutants, relative to the wild-type protein. The flexibility of the binding loop is increased in both R50A- and R52A-rCMTI-V. In R52A-rCMTI-V, the mean generalized order parameter ($<S^2>$) of the P_6-P_1 residues of the binding loop (39−44) decreases to 0.68 ± 0.02 from 0.76 ± 0.04 observed for the wild-type protein. However, in R50A-rCMTI-V, the flexibility of the whole binding loop increases, especially that of the $P_1'-P_3'$ residues (45−47), whose $<S^2>$ value drops dramatically to 0.35 ± 0.03 from 0.68 ± 0.03 determined for rCMTI-V. More strikingly, S^2 values of side-chain NϵHs reveal that, in the R50A mutant, removal of the R50 hydrogen bond results in the loss of the R52 hydrogen bond too, whereas in R52A, the R50 hydrogen bond remains unaffected. Kinetic data on trypsin-catalyzed hydrolysis of the reactive-site peptide bond (P_1-P_1') suggest that the activation free energy barrier of the reaction at 25 °C is reduced by 2.1 kcal/mol for R50A-rCMTI-V and by 1.5 kcal/mol for R52A-rCMTI-V, relative to rCMTI-V. Collectively, the results suggest that although both the P_6' and P_8' anchors are required for optimal inhibitor function and stability in the potato I family, the former is essential for the existence of the latter and has greater influence on the binding-loop structure, dynamics, and stability.

The binding-loop conformation of a serine protease protein inhibitor is supported by a network of hydrogen-bonding and hydrophobic interactions, including disulfide bridges, and different inhibitor families exhibit distinct combinations of these protein scaffold−binding loop interactions (*1*). Many studies have characterized the dominant effects of binding-loop residues (P_6-P_4'; nomenclature as per ref *2*) on the side chain−side chain interactions in cognate enzyme−inhibitor complexes and their influence on inhibitor function (refs *3*−*5*, for example). These canonical inhibitors act as "slow substrates"(*6*); therefore, assessment of relative contributions of various binding loop−protein scaffold interactions to inhibitor stability and function is of importance for the designing of efficacious novel inhibitors. The role of an asparagine residue in the stability of the reactive-site loop of the soybean trypsin inhibitor family has recently been demonstrated (*7*). In the case of the potato I family of inhibitors, the binding loop is anchored to the protein scaffold via hydrogen bonds, one on either side of the reactive-site peptide bond ($P_1-P_{1'}$), by two arginine residues at the P_6' and P_8' positions (*8*−*11*). Interestingly, in *Linum usitatissimum* trypsin inhibitor (LUTI),[1] a tryptophan, replacing arginine at P_8', supports the Pn segment of the binding loop (*12*). Thus, a potato I family inhibitor provides a simple, but useful, system to explore and characterize structural and dynamic effects of scaffold−binding loop anchors and their impact on inhibitor stability and function.

We have carried out extensive structural and dynamic studies of *Cucurbita maxima* trypsin inhibitor-V (CMTI-V; 7.4 kD; *13*), a potato I family member and a specific inhibitor

† This work was supported by grants from the National Institutes of Health (HL-40789) and the American Heart Association, Kansas Affiliate. R.K. was supported by an NIH Research Career Development Award (HL-03131). This is contribution 02-445-J from the Kansas Agricultural Experiment Station.

* To whom correspondence should be addressed. Phone: (785) 532-6262. Fax: (785) 532-7278. E-mail: krish@ksu.edu.

‡ Kansas State University.

§ Present address: Laboratory of Chemical Physics, National Institutes of Health, Bethesda, MD 20892.

⊥ Western Illinois University.

10.1021/bi0258952 CCC: $22.00
Published on Web 07/03/2002

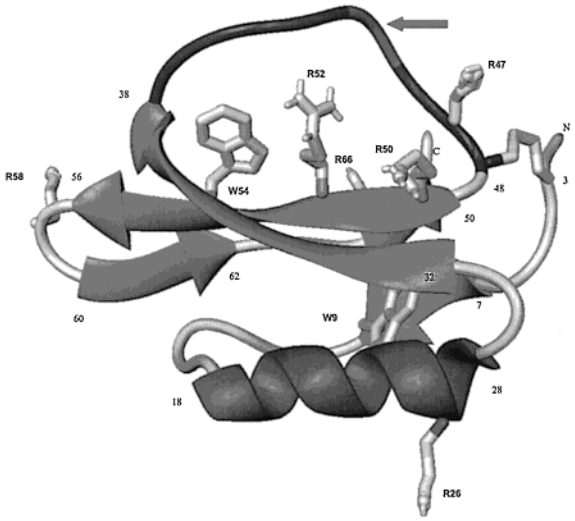

FIGURE 1: NMR solution structure of rCMTI-V (*15*), depicting the side chains of arginine and tryptophan side chains. Arg[50] and Arg[52] anchor the binding loop to the protein scaffold through hydrogen-bonding interactions. The arrow indicates the scissile peptide bond ($P_1-P_{1'}$) between Lys[44] and Asp[45] (*13*). Only the main-chain atoms of other residues are shown.

Table 1: Thermodynamic Parameters of Thermal Denaturation of rCMTI-V and Mutants, R50A and R52A[a]

protein	T_m (°C)	ΔH_m (kcal/mol)	ΔC_p (kcal/(mol·K))	$\Delta H_d^{25°C}$ (kcal/mol)	$\Delta G_d^{25°C}$ (kcal/mol)	$\Delta\Delta G_d^{25°C}$ (kcal/mol)
rCMTI-V	70.9	63.5	0.42	44.2	7.0	
R50A	62.6	31.2	0.13	26.4	3.1	−3.9
R52A	65.7	43.5	0.24	33.7	4.8	−2.2

[a] Data taken from ref *18*.

of human factor XIIa-a serine protease that initiates the intrinsic pathway of clot formation (*14*). In CMTI-V, Arg[50] and Arg[52] side chains provide the scaffold support to the binding loop by means of hydrogen bonds (Figure 1; *15*). In addition, the binding loop is connected to the protein core by a Cys[3]−Cys[48] cross-link. The arginine hydrogen bonds are stable, even at pH 2.5 (*16*) and are retained in the reactive-site (Lys[44]−Asp[45]) hydrolyzed form of the inhibitor (*16*, *17*). Replacement of Arg[50] or Arg[52] by either alanine, lysine, or glutamine decreases the inhibitor's stability toward proteolysis by trypsin, with the R50 mutants showing more pronounced effects than their R52 counterparts (*16*). Thermal denaturation studies reveal that R50A is more destabilized than R52A relative to the wild-type protein (Table 1; *18*). These results bring forth the following questions. How is the binding-loop stability affected by the protein scaffold? Do the binding-loop anchors have an effect on the structure and stability of the protein scaffold as well? What are the differences between the two hydrogen-bond anchors in terms of structural and dynamic consequences?

[1] Abbreviations: LUTI, *Linum usitatissimum* trypsin inhibitor; CMTI-V, *Cucurbita maxima* trypsin inhibitor-V; rCMTI-V, recombinant *Cucurbita maxima* trypsin inhibitor-V; CMTI-V*, reactive-site hydrolyzed *Cucurbita maxima* trypsin inhibitor-V; RP-HPLC, reversed-phase high-pressure liquid chromatography; NMR, nuclear magnetic resonance; NOE, nuclear Overhauser effect; HSQC, heteronuclear single quantum coherence; HMQC, heteronuclear multiple quantum coherence; DQF-COSY, double-quantum filtered correlated spectroscopy; TOCSY, total correlated spectroscopy; NOESY, nuclear Overhauser effect spectroscopy; CPMG, Carr−Purcell−Meiboom−Gill; SD, standard deviation; ppm, parts per million; CI-2, chymotrypsin inhibitor-2.

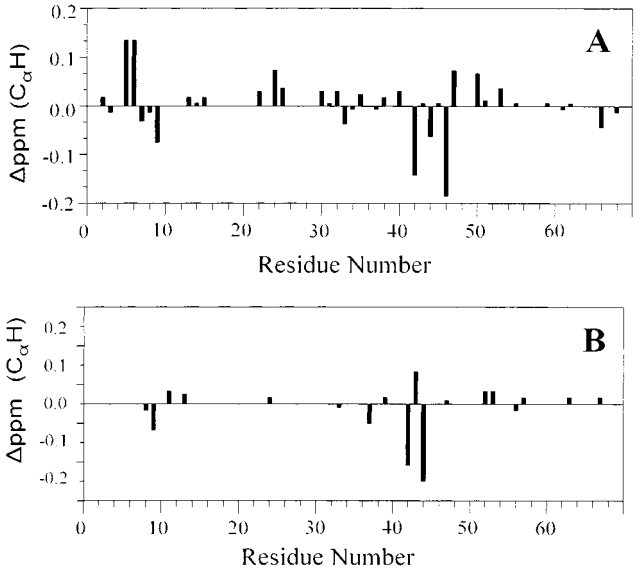

FIGURE 2: Plots of $C_\alpha H$ hydrogen chemical shift differences (mutant − wild type) as a function of residue number: (A) R50A-rCMTI-V; (B) R52A-rCMTI-V. For clarity, values equal to or greater than the error limit of ±0.03 ppm alone are shown.

Herein we present NMR studies of R50A- and R52A-rCMTI-V which demonstrate that, while structural perturbations of the substitutions are minimal, the backbone mobility of the binding loop is greatly enhanced by the R50A, rather than the R52A, swap. Determination of side-chain dynamics reveals a more important structural and functional role for Arg[50]: in R50A, the Arg[52] anchor is also lost, whereas in R52A, the Arg[50] hydrogen bond is retained. Kinetic data of trypsin-catalyzed hydrolysis of R50A- and R52A-rCMTI-V indicate that increased flexibility of the Pn′ segment of the binding loop is largely responsible for the inhibitor's decreased affinity toward trypsin and increased susceptibility to proteolysis.

MATERIALS AND METHODS

Proteins. Recombinant proteins, rCMTI-V, R50A-rCMTI-V, and R52A-rCMTI-V, were expressed in *Escherichia coli* and purified, as described (*16*, *19*). Uniformly ^{15}N-labeled R50A- and R52A-rCMTI-V needed for NMR studies were prepared from *E. coli* cells grown in a medium containing $^{15}NH_4Cl$. For NMR experiments, approximately 3 mM ^{15}N-labeled R50A-rCMTI-V and R52A-rCMTI-V solutions were prepared in 90% H_2O/10% D_2O (v/v) that contained 50 mM KCl at pH 5.0.

NMR Spectroscopy. NMR experiments were performed at 30 °C with a 11.7 T (500 MHz for ^1H) Varian UNITYplus instrument. Data processing and analyses were carried out with Varian VNMR software (version 5.1). DQF-COSY, TOCSY, NOESY, and ^{15}N-edited HSQC-TOCSY data sets were collected using a spectral width of 7000 Hz over 2K data points and 256 increments, using the standard pulse sequences (*20*). The data matrix was zero-filled to 4K × 4K and processed. The reported ^1H chemical shifts are relative to 4.71 ppm assigned to the H_2O peak at 30 °C. The ^{15}N chemical shifts are relative to CH_3NO_2 which was assigned a ^{15}N chemical shift of 380.23 ppm from liquid NH_3 (*21*).

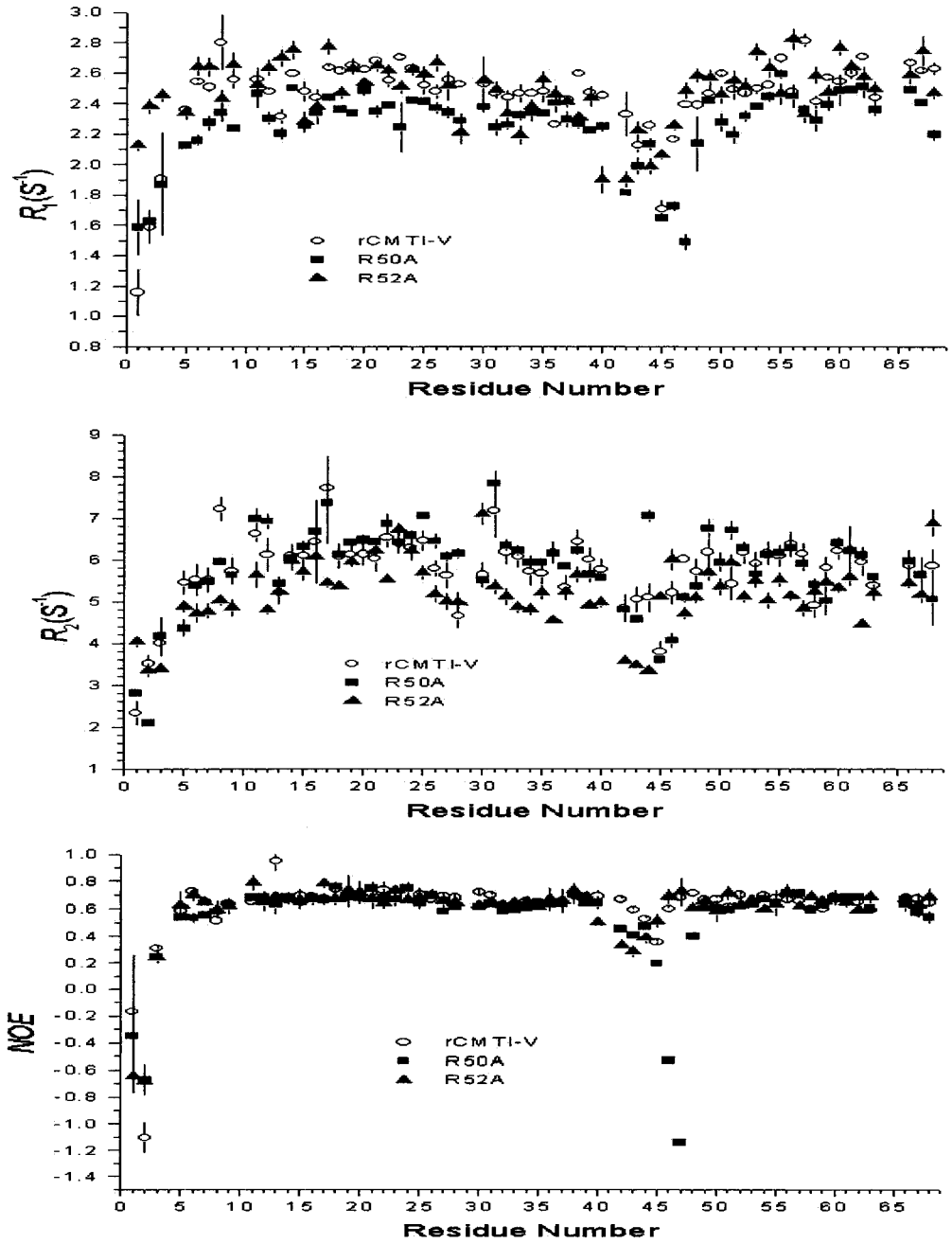

FIGURE 3: Plots of ^{15}N relaxation parameters, R_1, R_2, and NOE, of main-chain NH groups as a function of residue number for rCMTI-V and the mutants, R50A and R52A, at pH 5.0, 30 °C. The data for rCMTI-V are taken from ref *16*.

^{15}N Relaxation Measurements and Analysis. Spin-lattice and spin-relaxation rate constants (R_1 and R_2, respectively) and $^1H-^{15}N$ steady-state NOEs were measured using inversion−recovery, Carr−Purcell−Meiboom−Gill (CPMG), and steady-state NOE experiments, respectively, as described previously (*22*); sensitivity-enhanced proton-detected $^1H-^{15}N$ heteronuclear 2D pulse sequences (*23*) were used. Data processing was carried out as described (*16*). The ^{15}N relaxation data, including R_1, R_2, and NOE, were analyzed according to the model-free formalism (*24*), using the software, Model Free (version 3.0). The average R_2/R_1 ratio of all main-chain and side-chain NH groups was calculated, and the ones with less than one standard deviation from the average value were selected to estimate and optimize the overall tumbling time, τ_m (*25*). Generalized order parameter, S^2, effective internal correlation time, τ_e, and the chemical exchange term, Δ_{ex}, were calculated simultaneously for all NHs at a fixed τ_m, (*25*).

Kinetics of Proteolysis of rCMTI-V, R50A-rCMTI-V, and R52A-rCMTI-V by Trypsin. Trypsin-catalyzed hydrolysis of rCMTI-V and the mutants was followed as a function of time by reversed-phase high-pressure liquid chromatography (RP-HPLC). The reaction mixture consisted of 5 mol % trypsin mixed with a given inhibitor in 50 mM potassium phosphate buffer (pH 6.75) at room temperature (300 K). Aliquots were withdrawn at various time intervals and analyzed by RP-HPLC to monitor the relative levels of the intact inhibitor (I) and the reactive-site hydrolyzed form (I*). A C18 column and an eluent mixture of water containing 0.1% (v/v) trifluoroacetic acid (solvent A) and acetonitrile mixed with 0.1% (v/v) trifluoroacetic acid (solvent B) were used. The composition of the eluent mixture was changed

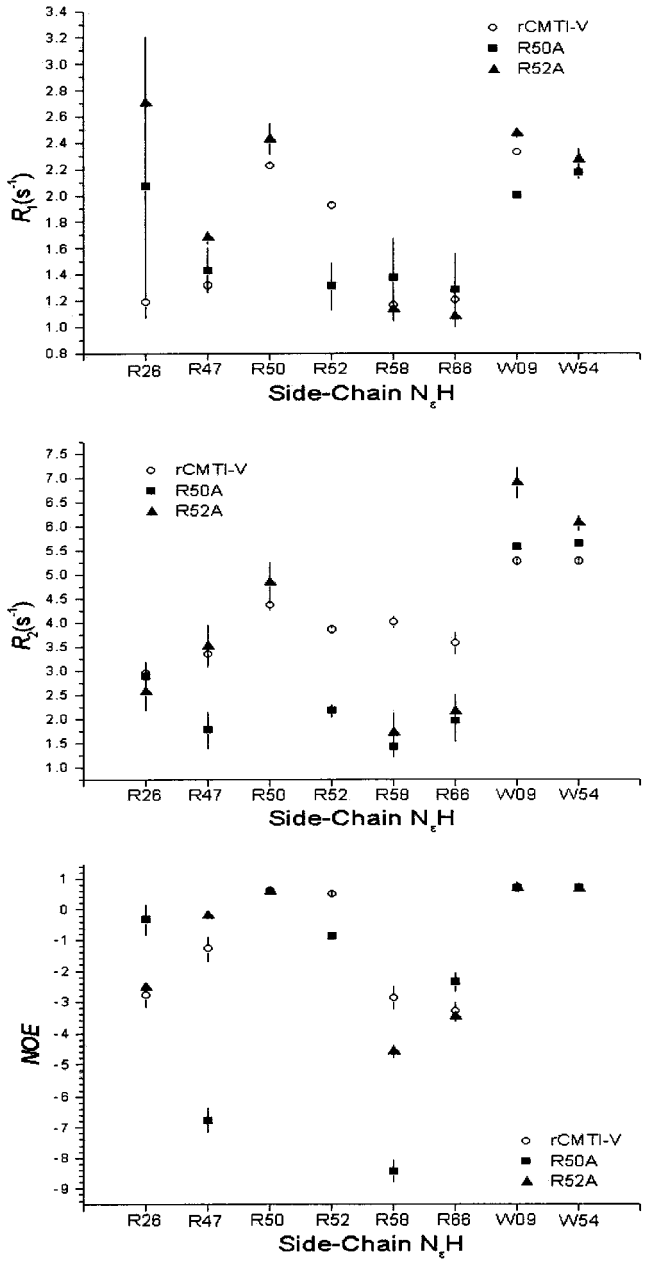

FIGURE 4: Plots of ^{15}N relaxation parameters, R_1, R_2, and NOE, of side-chain NϵHs of arginine and tryptophan residues in rCMTI-V and the mutants, R50A and R52A, at pH 5.0, 30 °C. The data for rCMTI-V are taken from ref *16*.

from 20% B to 100% B in a period of 40 min. Peak areas were determined by integration using a Varian HPLC software (Star Chromatography, version 4.0). In some cases, peak heights were used. The rate of disappearance of the intact form (I) of the inhibitor was followed. Assuming a pseudo-first-order rate law, which is applicable to the formation of I* from the slow breakdown of trypsin−intact inhibitor (E:I) complex (*26*), the half-life of the reaction, $t_{1/2}$, during which 50% of the intact inhibitor was hydrolyzed, was calculated.

RESULTS AND DISCUSSION

^1H and ^{15}N Resonance Assignments. All main-chain ^{15}N and ^1H resonances and most of the side-chain hydrogens were assigned for R50A- and R52A-rCMTI-V (Tables S-1A and S-1B; Supporting Information), following the standard 2D NMR strategies (*27*). The NMR assignment procedures developed for natural CMTI-V (*11*) and rCMTI-V (*15*, *16*) were followed. Sequential $^1H-^1H$ NOEs obtained from a 100 ms NOESY map (not shown) were used to identify the secondary structures. The ^{15}N and ^1H chemical shifts of backbone NH groups are influenced by factors, such as hydrogen bonding and solvent accessibility, besides protein conformation (*28*). Therefore, we have relied upon the $C_\alpha H$ hydrogen chemical shift comparison as a structural probe (Figure 2). In the case of R50A-rCMTI-V, besides the binding-loop residues, 42−47, some residues located in the N-terminal, α-helical (18−28), β-sheet (32−28), and turn (28−31) regions are also perturbed (Figure 2A). However, comparison of sequential $^1H-^1H$ NOE cross-peaks of the wild-type protein and the mutant reveals no differences for any of the secondary structure elements. Similarly, the long-range NOEs identified for the R50A variant are not different from those identified for rCMTI-V (data not shown). These results suggest that, aside from some minor structural alterations, the overall three-dimensional structure of the R50A mutant is very similar to that of rCMTI-V. In the case of R52A-rCMTI-V, only the binding-loop residues, 42−44, report significant chemical shift changes (Figure 2B). No differences were observed between the wild-type protein and the mutant in either sequential or long-range NOE cross-peak patterns (not shown). Accordingly, we deduce that the overall three-dimensional structure of rCMTI-V is not changed by the R52A mutation.

Table 2: Comparison of Mean Generalized Order Parameters ($<S^2>$) of Secondary Structure Elements in rCMTI-V, R50A-rCMTI-V, and R52A-rCMTI-V

			mean generalized order parameters $<S^2>$		
secondary structure	sequence	no. of residues	rCMTI-V[a]	R50A-rCMTI-V	R52A-rCMTI-V
α	18−28	11	0.88 ± 0.01	0.82 ± 0.06	0.85 ± 0.07
β1	7−9	3	0.84 ± 0.07	0.77 ± 0.02	0.83 ± 0.06
β2	32−38	7	0.82 ± 0.04	0.84 ± 0.04	0.83 ± 0.05
β3	51−56	6	0.85 ± 0.03	0.86 ± 0.04	0.84 ± 0.06
β4	54−56	3	0.86 ± 0.02	0.86 ± 0.03	0.84 ± 0.04
β5	60−62	3	0.88 ± 0.03	0.86 ± 0.04	0.85 ± 0.04
β6	65−67	3	0.89 ± 0.01	0.83 ± 0.01	0.83 ± 0.03
T(I)	12−15	4	0.84 ± 0.06	0.80 ± 0.03	0.87 ± 0.07
T(IIa)	28−31	4	0.85 ± 0.01	0.79 ± 0.03	0.78 ± 0.04
T(IIb)	**47−50**	**4**	**0.85 ± 0.03**	**0.60 ± 0.08**	**0.80 ± 0.02**
T(III)	57−60	4	0.86 ± 0.06	0.82 ± 0.05	0.83 ± 0.03
binding loop	39−44	6	0.76 ± 0.04	0.69 ± 0.03	0.68 ± 0.02
	45−47	3	0.68 ± 0.03	0.35 ± 0.03	0.66 ± 0.03

[a] Taken from ref *16*.

Chemical shifts were also compared for Trp^9 and Trp^{54} ring hydrogens in rCMTI-V, R50A-rCMTI-V, and R52A-rCMTI-V (Tables S-1A and S-1B; Supporting Information), and no major differences were observed. Trp^9 is located in a hydrophobic pocket and has van der Waals contacts with the α-helix residues Ile^{24}, Gln^{27}, and Asn^{28} and the β-sheet residues Val^{51}, Pro^{65}, Arg^{66}, and Ile^{67} (*11*). The unchanged chemical shifts of Trp^9 ring hydrogens in the two mutant inhibitors indicate preservation of the scaffold structure. The Trp^{54} ring extensively interacts with the first half of the binding-loop Leu^{36}, Glu^{37}, Glu^{38}, Thr^{40}, and Val^{42} (*11*). In addition, its Nϵ atom forms a hydrogen bond with the main-chain oxygen of Arg^{52} (*15*). Thus, the unaltered chemical shifts of Trp^{54} ring hydrogens argue against significant

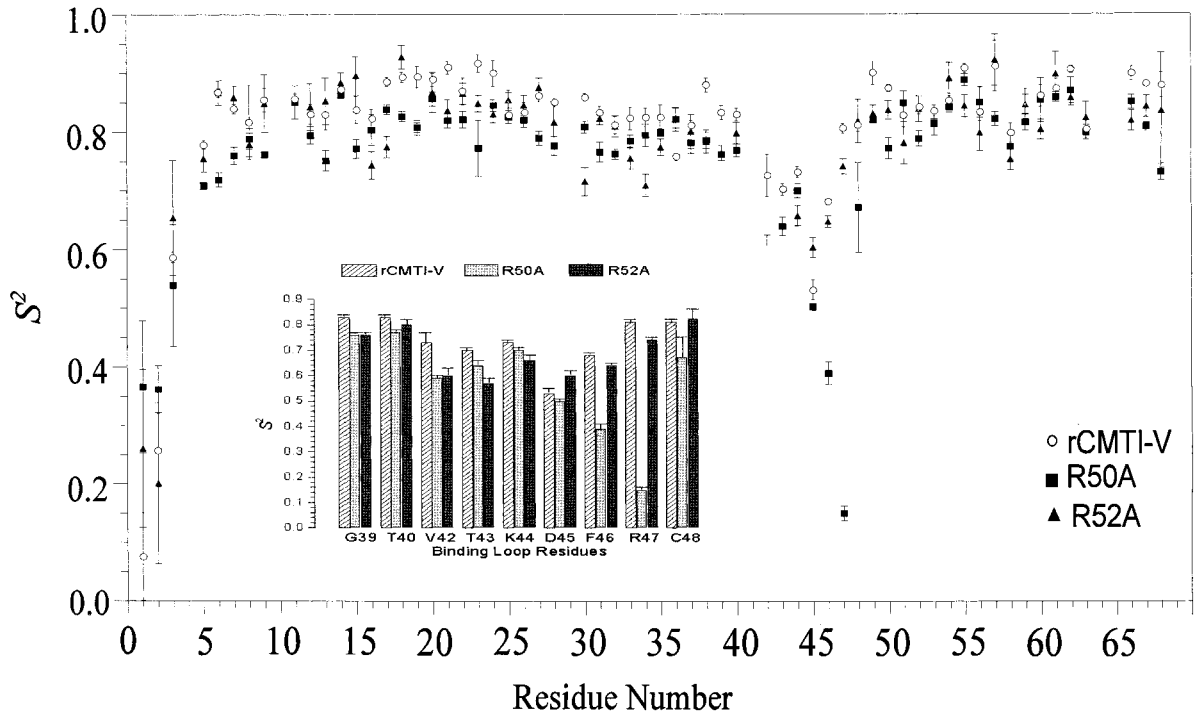

FIGURE 5: Comparison of generalized order parameter (S^2) values of backbone NH groups of R50A-rCMTI-V, R52A-rCMTI-V, and rCMTI−V. The data for the wild-type inhibitor are taken from ref *16*. The inset shows a comparative bar graph of S^2 values of the binding-loop residues in the three proteins for the purpose of clarity.

conformational changes of the binding loop in R50A- and R52A-rCMTI-V, as compared to the wild-type protein.

Relaxation Measurements of NH Groups in R50A- and R52A-rCMTI-V. ^{15}N NMR relaxation parameters, R_1, R_2, and NOE, were measured for 69 NH groups in R50A- and R52A-rCMTI-V (Tables S-2A and S-2B; Supporting Information). These include 62 main-chain units (Figure 3) and seven side-chain units from five arginine and two tryptophan residues (Figure 4). For R50A-rCMTI-V, an average R_2/R_1 ratio of 2.544 ± 0.216 was computed from 54 main-chain NHs (only the ones with the R_2/R_1 ratio difference of less than 1 SD from the average value were selected), and the overall tumbling time, τ_m, was optimized at 4.717 ± 0.013 ns. For R52A-rCMTI-V, an average R_2/R_1 ratio of 2.108 ± 0.220 was computed from 54 main-chain NHs, and τ_m was optimized at 3.816 ± 0.018 ns. The τ_m obtained for rCMTI-V under similar experimental conditions was 4.40 ± 0.020 ns (*16*). The different overall tumbling times determined for the two mutants likely arise from differences in their hydration properties, as observed for rCMTI-V at two different pH's (*16*). rCMTI-V, R50A-rCMTI-V, and R52A-rCMTI-V exhibit very different retention times on the RP-HPLC (*16*), thus indicating their varying hydrophobicities. This is corroborated by the fact that these mutants exhibit quite different ΔC_p values of thermal denaturation (Table 1; *18*), a measure of relative hydration of the folded state (*29*).

The computed generalized order parameters, S^2, internal correlation time, τ_e, and the exchange term, Δ_{ex}, for both main-chain and side-chain NHs of R50A-rCMTI-V and R52A-rCMTI-V are given in the Supporting Information (Tables S-3A and S-3B). Under the model-free formalism (*24*), only S^2 values are interpretable in terms of flexibility. Thus, in Figure 5, we compare S^2 values of main-chain NHs of R50A- and R52A-rCMTI-V with those of rCMTI-V (*16*). As expected from our earlier work (*15*, *16*), these values

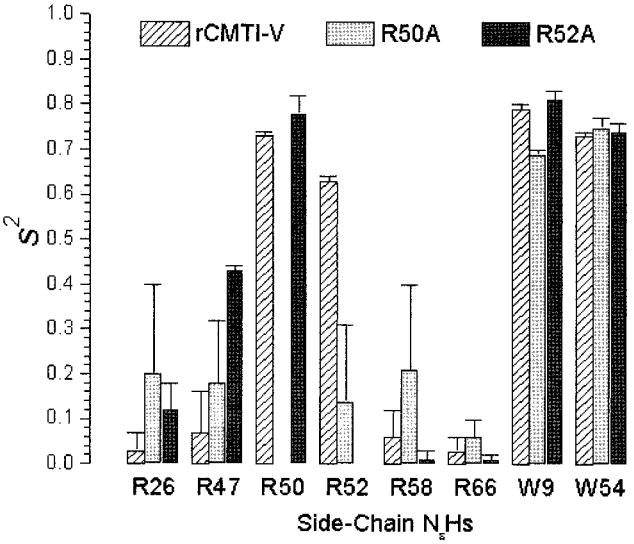

FIGURE 6: Comparative bar graphs of S^2 values of side-chain $N_\epsilon H$ groups of arginine and tryptophan residues in rCMTI-V, R50A-rCMTI-V, and R52A-rCMTI-V. The data for the wild-type protein are taken from ref *16*.

are high for most of the main-chain NHs, except the binding loop and N-terminal segment. Mean S^2 values are of the secondary structure elements are compared among the three proteins in Table 2. Only the turn made up of residues 47−50 [T(IIb)] becomes more flexible and, that too, only in the R50A mutant. This suggests that the overall scaffold structures of the two mutants remain very similar to that of the wild-type protein.

In contrast, the binding-loop flexibility increases in both R50A- and R52A-rCMTI-V, as would be anticipated from the removal of any of the two hydrogen bonds that bridge the binding loop and the protein core. Comparison of the S^2 values of the binding-loop residues (39−47; P_6-P_3') in the

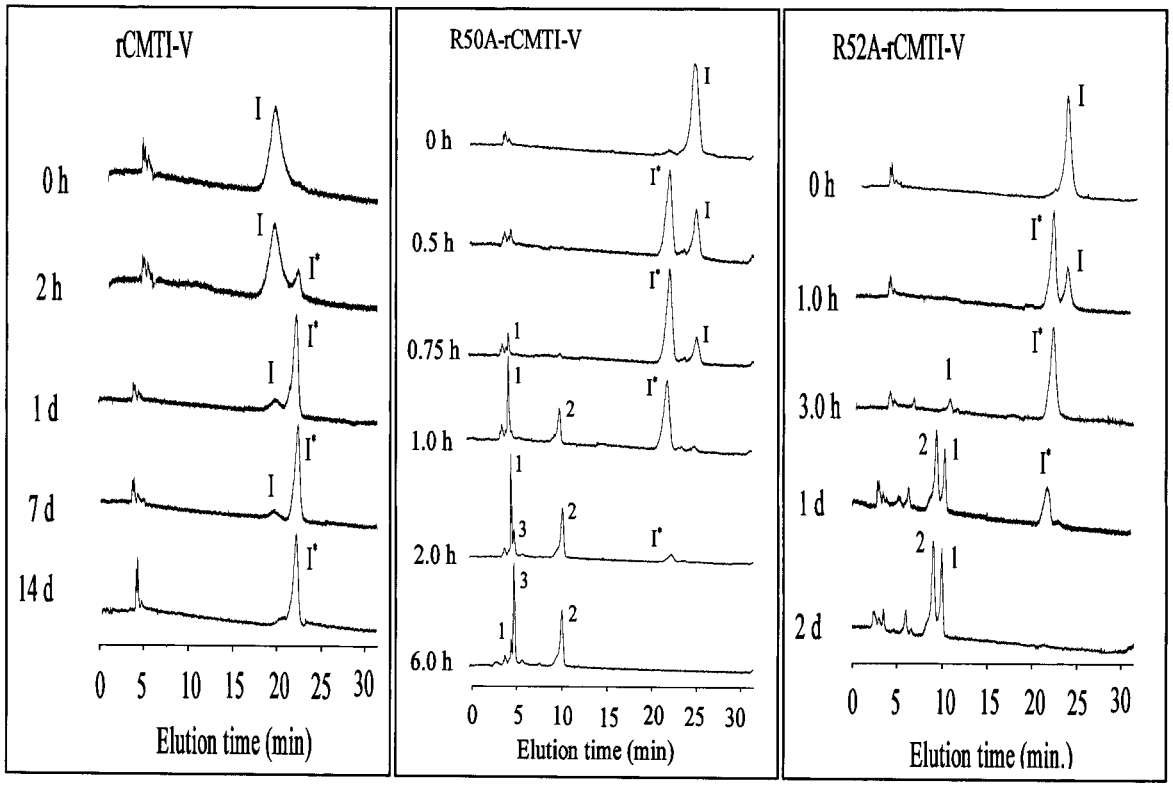

FIGURE 7: RP-HPLC traces of rCMTI-V, R50A-rCMTI-V, and R52A-rCMTI-V incubated separately with 5 mol % trypsin at 25 °C, pH 6.75. Aliquots were withdrawn at different times, as indicated and analyzed by RP-HPLC, using optical detection at 280 nm. I represents the intact inhibitor and I* the reactive-site ($Lys^{44}-Asp^{45}$) hydrolyzed inhibitor. The numbered peaks arise from fragments that result from further hydrolysis of I*. Half-life periods of I were calculated from the rate of decrease of peak area or intensity.

wild-type and two mutant proteins (inset in Figure 5), however, reveals a dramatic picture. In R52A-rCMTI-V, flexibility of the Pn portion of the binding loop (residues 39−44) increases slightly, whereas in R50A-rCMTI-V, flexibility of the whole loop, especially its Pn′ segment (residues 45−47), increases significantly (Table 2). Binding-loop residues have been found to contribute to protein global stability in the case of chymotrypsin inhibitor 2 (CI-2), another potato I family member (*30*).

Side-Chain Dynamics of Arginine and Tryptophan Residues. S^2 values of side-chain NH groups (Nϵ-Hs) of arginine and tryptophan residues are compared in Figure 6 (Tables S-4A and S-4B; Supporting Information). Both Trp^9 and Trp^{54} side chains remain rigid in R50A- and R52A-rCMTI-V with the Trp^9 ring gaining a little mobility in R50A-rCMTI-V. Trp^9 ring atoms have close contacts with the N-terminal segment, which is connected to the second half of the binding loop through the Cys^3-Cys^{48} bridge (*11*). Thus, increased mobility of the binding loop due to the R50A swap brings about a similar effect on Trp^9. The unchanged internal mobility of Trp^{54} indicates retention of its hydrophobic interactions with the binding-loop residues 36−42.

Among arginine side chains, Arg^{26}, Arg^{47}, Arg^{58}, and Arg^{66} remain flexible in both R50A- and R52A-rCMTI-V (Figure 6). Arg^{50} and Arg^{52} side chains are rigid in rCMTI-V, as they are hydrogen-bonded to the binding loop (*16*). However, in R50A-rCMTI-V, the S^2 value of Arg^{52} NϵH drops considerably, to the level of a flexible side chain. This indicates that the hydrogen-bonding interaction between the Arg^{52} side chain and the binding loop is abolished. Accordingly, increased flexibility is experienced by the hydrogen-bond acceptor residues 46 and 47 in R50A-rCMTI-V (inset in Figure 5). In sharp contrast, in R52A-rCMTI-V the Arg^{50} side-chain retains its rigidity and, hence, its hydrogen-bonding interaction with the binding loop. Thus, we conclude that the Arg^{50} anchor is required for the formation of the Arg^{52} anchor. The present results also offer an explanation for the observed relative thermal stabilities of the two mutants (Table 1; *18*): R50A is 1.7 kcal/mol less stable than R52A at 25 °C and its melting temperature is 3.1 °C lower. The P_8' arginine contributes 1.4 kcal/mol to stability (to chemical denaturation) in CI-2 (*31*) and 2.2 kcal/mol at 25 °C to thermal stability in rCMTI-V (*18*).

The current study reveals effects that extend beyond the residue that is replaced. Earlier thermodynamic studies of effects of single amino acid replacements in serine proteinase inhibitors have, in fact, identified several cases showing such nonlocal effects (*32*). However, lack of complete structural and dynamical information has precluded an explanation for the observations.

While arginine residues at P_6' and P_8' positions are generally well-conserved in the potato I family, the P8′ position is occupied by a tryptophan in LUTI, whose three-dimensional solution structure has been determined (*12*). The binding loop−scaffold interaction is preserved by a tryptophan hydrogen bond, and the shorter side chain at P_8' leads to a closer packing of the binding loop with the protein scaffold (*12*).

Trypsin-Catalyzed Proteolysis of rCMTI-V, R50A-rCMTI-V, and R52A-rCMTI-V. Trypsin specifically cleaves the $Lys^{44}-Asp^{45}$ peptide bond (P_1-P_1') of the inhibitor (I) to produce the clipped form, I* in a slow step, following the

rapid formation of trypsin−inhibitor complex. Figure 7 shows RP-HPLC data reflecting the stability of rCMTI-V and the mutants, R50A and R52A, toward trypsin. From the rate of decrease of peak intensity or area of I, half-life periods ($t_{1/2}$) of the enzyme−inhibitor complex are estimated to be 6.3×10^2, 17, and 48 min for rCMTI-V, R50A-rCMTI-V, and R52A-rCMTI-V, respectively. It is of interest to recall that, in the case of rCMTI-V*, the reactive-site hydrolyzed wild-type protein, the two anchoring hydrogen bonds are still intact (*17*), thus protecting the clipped inhibitor from further proteolysis for more than a week. From the kinetic data (Figure 7), it is calculated that the activation free energy barrier of the specific hydrolysis at 25 °C is reduced by 2.14 kcal/mol for R50A and by 1.52 kcal/mol for R52A, relative to rCMTI-V (*33*). Thermal denaturation data indicate that, at 25 °C, R50A is destabilized by 3.9 kcal/mol and R52A by 2.2 kcal/mol, relative to the wild-type protein (Table 1; *18*, *34*). From these two sets of data, we may infer decreased binding affinities for the mutants, as that would account for an elevated free energy of the transition state consisting of the E:I complex and, hence, a higher activation free energy barrier (*35*). Indeed, the following decreasing order of trypsin-binding affinity is observed: rCMTI-V > R52A > R50A (*34*).

CONCLUSIONS

Of the two hydrogen-bond supports to the binding loop provided by the side chains of Arg^{50} and Arg^{52} at P_6' and P_8' positions, respectively, in CMTI-V, the former contributes more to inhibitor function and stability. While structural changes due to removal of these hydrogen bonds by the R/A substitution are minimal, significant differences occur in the internal dynamics of the mutants. Abrogation of the Arg^{50} anchor also results in the loss of the Arg^{52} hydrogen bond and leads to significantly enhanced internal mobility of the Pn′ segment of the binding loop. In contrast, removal of the Arg^{52} hydrogen bond does not affect the Arg^{50} support and raises the flexibility of the Pn segment only slightly. Thus, although both P_6' and P_8' anchors are essential for optimal stability and function of the potato I family of inhibitors, the former is required for the existence of the latter, and its removal results in a greater loss of trypsin-binding affinity and proteolytic stability.

ACKNOWLEDGMENT

We thank Y. Huang, J. Liu, O. Prakash, J.-K. Huang, and S.P. Dunkelbarger for technical assistance at various stages of the project.

SUPPORTING INFORMATION AVAILABLE

Two figures and eight tables containing ^1H and ^{15}N assignments of R50A- and R52A-rCMTI-V at pH 5.0, experimental R_1, R_2, and NOE measurements, and calculated model-free parameters (S^2, τ_e, and Δ_{ex}) for main-chain and side-chain NHs of R50A- and R52A-rCMTI-V at pH 5.0. This material is available free of charge via the Internet at http://pubs.acs.org.

REFERENCES

1. Bode, W., and Huber, R. (1992) *Eur. J. Biochem. 204*, 433−451.
2. Schechter, I., and Berger, M. (1967) *Biochem. Biophys. Res. Commun. 27*, 157−162.
3. Qasim, M. A., Ganz, P. J., Saunders, C. W., Bateman, K. S., James, M. N., and Laskowski, M., Jr. (1997) *Biochemistry 36*, 1598−1607.
4. Lu, S. M., Lu, W., Qasim, M. A., Anderson, S., Apostol, I., Ardelt, W., Bigler, T., Chiang, Y. W., Cook, J., James, M. N., Kato, I., Kelly, C., Kohr, W., Komiyama, T., Lin, T. Y., Ogawa, M., Otlewski, J., Park, S. J., Qasim, S., Ranjbar, M., Tashiro, M., Warne, N., Whatley, H., Wieczorek, A., Wieczorek, M., Wilusz, T., Wynn, R., Zhang, W., and Laskowski, M., Jr. (2001) *Proc. Natl. Acad. Sci. U.S.A. 98*, 1410−1415.
5. Otlewski, J., Jaskolski, M., Buczek, O., Cierpicki, T., Czapinska, H., Krowarsch, D., Smalas, A. O., Stachowiak, D., Szpineta, A., and Dadlez, M. (2001) *Acta Biochim. Pol. 48*, 419−428.
6. Laskowski, M., Jr., and Kato, I. (1980) *Annu. Rev. Biochem. 49*, 593−626.
7. Ravichandran, S., Dasgupta, J., Chakrabarti, C., Ghosh, S., Singh, M., and Dattagupta, J. K. (2001) *Protein Eng. 14*, 349−357.
8. McPhalen, C. A., and James, M. N. G. (1987) *Biochemistry 26*, 261−269.
9. Clore, G. M., Gronenborn, A. M., James, M. N. G., Kjaer, M., McPhalen, C. A., and Poulsen, F. M. (1987) *Protein Eng. 1*, 313−318.
10. Hyberts, S. G., Goldberg, M. S., Havel, T. F., and Wagner, G. (1992) *Protein Sci. 1*, 736−751.
11. Cai, M., Gong, Y., Kao, J. L. F., and Krishnamoorthi, R. (1995) *Biochemistry 34*, 5201−5211.
12. Cierpicki, T., and Otlewski, J. (2000) *J. Mol. Biol. 302*, 1179−1192.
13. Krishnamoorthi, R., Gong, Y., and Richardson, M. (1990) *FEBS Lett. 273*, 163−167.
14. Pixley, R. A., and Colman, R. W. (1993) *Methods Enzymol. 222*, 51−65.
15. Liu, J., Prakash, O., Cai, M. L., Gong, Y., Huang, Y., Wen, L., Wen, J. J., Huang, J. K., and Krishnamoorthi, R. (1996) *Biochemistry 35*, 1516−1524.
16. Cai, M., Huang, Y., Prakash, O., Wen, L., Dunkelbarger, S. P., Huang, J. K., Liu, J., and Krishnamoorthi, R. (1996) *Biochemistry 35*, 4784−4794.
17. Liu, J., Prakash, O., Huang, Y., Wen, L., Wen, J. J., Huang, J. K., and Krishnamoorthi, R. (1996) *Biochemistry 35*, 12503−12510.
18. Zavodszky, M., Chen, C.-W., Huang, J.-K., Zolkiewski, M., Wen, L., and Krishnamoorthi, R. (2001) *Protein Sci. 10*, 149−160.
19. Wen, L., Kim, S. S., Tinn, T. T., Huang, J. K., Krishnamoorthi, R., Gong, Y. X., Lwin, Y. N., and Kyin, S. (1993) *Protein Expression Purif. 4*, 215−222.
20. Frenkiel, T. A. (1995) in *NMR of Macromolecules: A Practical Approach* (Roberts, G. C. K., Ed.), pp 35−70, IRL Press, Oxford, U.K.
21. Live, D. H., Davis, D. G., Agosta, W. C., and Cowburn, D. (1984) *J. Am. Chem. Soc. 106*, 6104−6105.
22. Kay, L. E., Torchia, D. A., and Bax, A. (1989) *Biochemistry 28*, 8972−8979.
23. Skelton, N. J., Palmer, A. G., III, Akke, M., Kördel, J., Rance, M., and Chazin, W. J. (1993) *J. Magn. Reson., Ser. B 102*, 253−264.
24. Lipari, G., and Szabo, A. (1982) *J. Am. Chem. Soc. 104*, 4559−4570.
25. Clore, G. M., Driscoll, P. C., Wingfield, P. T., and Gronenborn, A. M. (1990) *Biochemistry 29*, 7387−7401.
26. Tinoco, I., Jr., Sauer, K., Wang, J. C., and Puglisi, J. D. (2002) *Physical Chemistry: Principles and Applications in Biological Sciences*, Prentice Hall, New York.
27. Wuethrich, K. (1986) *NMR of Proteins and Nucleic Acids*, Wiley-Interscience, New York.
28. Oldfield, E. (1995) *J. Biomol. NMR 5*, 217−225.
29. Privalov, P. L., and Makhatadze, G. I. (1992) *J. Mol. Biol. 224*, 715−723.
30. Jackson, S. E., and Fersht, A. R. (1994) *Biochemistry 33*, 13880−13887.
31. Jandu, S. K., Ray, S., Brooks, L., and Leatherbarrow, R. J. (1990) *Biochemistry 29*, 6264−6269.
32. Ardelt, W., and Laskowski, M., Jr. (1991) *J. Mol. Biol. 220*, 1041−1053.
33. Lonhienne, T., Gerday, C., and Feller, G. (2000) *Biochim. Biophys. Acta 1543*, 1−10.

34. Zavodszky, M. (1999) Disulfide bond effects on protein stability: Designed variants of *Cucurbita maxima* trypsin inhibitor-V (CMTI−V). M.S. Thesis, Kansas State University, Manhattan, KS.

35. Fersht, A. R. (1985) *Enzyme structure and mechanism*, W. H. Freeman and Company, New York.

BI0258952